Evidences and significance of ancient deep incursion of meteoric freshwater in buried sandstones

Guanghui Yuan[1*], Jon Gluyas[2], Yingchang Cao[1] *,

(1. School of Geoscience, China University of Petroleum, Qingdao, China 266580;
2. Department of Earth Sciences, Durham University, Durham, DH1 3LE UK)

Abstract: We present an example of ancient deep incursion of meteoric freshwater in the buried Eocene Es3 sandstones in the Gaoliu area, Nanpu Sag, Bohaibay Basin, East China. The interpretation is based on information from several independent techniques, including detailed petrographic analysis, and testing of homogenization temperature (T_h) of aqueous fluid inclusions (AFIs) and in situ $\delta^{18}O$ compositions within quartz overgrowths. Feldspars were leached to form large amount of intragranular secondary pores with secondary minerals including a few quartz cements and kaolinite. Early-diagenetic calcite cement was leached to form intergranular pores without precipitation of late-diagenetic calcite cements in most sandstones. Mineral dissolution has occurred in an open geochemical system mainly since the uplift period, with burial depth of most sandstones deeper than 1000-1500m. Coupled high T_h (95～115°C) of AFI and low $\delta^{18}O_{(cement)}$ values (+17～+20‰) within the quartz overgrowths suggest that quartz cementation and feldspar dissolution occurred in presence of paleo-fluids with $\delta^{18}O_{(water)}$ values of -7～-2‰. The negative $\delta^{18}O_{(water)}$ values and significant volume difference between leach minerals and accompanying secondary minerals support ancient deep incursion of meteoric freshwater in the sandstones at approximately 2500-3000m with an temperature gradient of 3.2-3.5℃/100m.

Deep meteoric leaching reactions formed approximated 7-10% enhanced secondary porosities to improve reservoir quality. We believe that this is an excellent example of ancient deep incursion of meteoric water in buried sandstones, which verified that deep meteoric leaching can do occur and improve reservoir quality in sandstones with developed faults acting as flow route.

Key Words: quartz overgrowths, fluid inclusions; in situ oxygen isotope; deep incursion of meteoric freshwater, enhanced secondary pores.

INTRODUCTION

Secondary porosity, formed after dissolution of mineral grains and possibly cements, is important contributor to reservoir quality in buried sandstones (Dutton and Loucks, 2010; França et al., 2003; Wilkinson et al., 2014). These secondary pores was generally interpreted to be formed by meteoric freshwater leaching reactions at shallow depth (Bjørlykke and Jahren, 2012; Emery et al., 1990; França et al., 2003) or by deep burial leaching reactions related with acids generated from maturation of kerogen within source rocks (Schmidt and McDonald, 1979; Yuan et al., 2015) or deep hot water (Taylor, 1996). Although meteoric water flow into sedimentary basins may extend 2-3 km below sea level, most meteoric diagenetic alteration was suggested to occur beneath unconformities or at burial depths less than a few hundred meters (Aagaard, 1992; Bjørlykke and Jahren, 2012). Franca (2003) reported an example of meteoric water leaching in Botucatu sandstones from outcrops to burial depth of 1000-1500m, however, petrography evidences of mineral dissolution was identified mainly in sandstones shallower than 250m (França et al., 2003). Gluyas (1997) reported the incursion of meteoric water in buried Rotiegend sandstones during an uplift period in a poster presentation (Gluyas et al., 1997). No authigenic mineral assemblage representing open geochemical system, however, was identified in the Rotiegend sandstones. Up to the present day, there is virtually very few literatures with hard evidences documenting burial leaching reactions induced by ancient deep incursion (>1500m) of meteoric freshwater in buried sandstones

(França et al., 2003).

Stable isotope compositions of authigenic kaolinite have been used as the most important evidence to support meteoric diagenesis in sandstones (Kevin, 1995; Bird and Chivas, 1988). Without precipitation temperature, however, $\delta^{18}O$ compositions of kaolinite alone cannot define unique isotopic chemistry of paleo-fluids. Thus kaolinite can be interpreted to be formed in low temperature–negative $\delta^{18}O$ water system or in high temperature–positive $\delta^{18}O$ water system (Kevin, 1995). What's more, the kaolinite samples used for isotope analysis may be combinations of detrital kaolinite and authigenic kaolinite, or early formed kaolinite and late formed kaolinite. In this paper, the studied buried sandstones experienced extensive leaching of detrital feldspars and early-daigenetic calcite cement, and some simultaneous quartz overgrowths were luckily precipitated on detrital grains. Given that the quartz overgrowths captured small inclusions of the fluid from which the quartz precipitated, we have a precious opportunity to investigate the origin of paleo-fluids related to these diagenetic reactions.

The purposes of this article were to: (1) identify the ancient deep incursion of meteoric freshwater in buried sandstones through analyzing sandstone diagenetic petrography, coupled homogenization temperature (T_h) of aqueous fluid inclusions (AFI) and in situ $\delta^{18}O$ compositions within the quartz overgrowths; and (2) verify that deep meteoric leaching can form enhanced secondary pores to improve reservoir quality.

1 GEOLOGICAL BACKGROUND

The Nanpu (NP) Sag, an important hydrocarbon-producing subunit of Bohai Bay Basin, is located on the eastern coast of China and covers an area of approximately 2462 km^2. It is a rift lacustrine basin developed in the Late Jurassic through to the early Cenozoic on the basement of the North China platform. The Nanpu Sag is further subdivided into 12 secondary structural units (Fig. 1A) (Guo et al., 2013). The Gaoliu (GL) area (including the Gaoshangpu structural belt and the Liuzan structural belt) at the northern part of the Nanpu sag was constrained by the Xinanzhuang Fault, Baigezhuang Fault and Gaoliu Fault (Fig. 1). With an area of approximately 200 km^2 (Zhang et al., 2008), the GL area is the objective area of this study.

From base to top, the sediments deposited in the Nanpu Sag are represented by the Shahejie (Es), the Dongying (Ed), Guantao (Ng), Minghuazhen (Nm), and Pingyuan (Q) formations (Fig. 1B) (Guo et al., 2013; Yuan et al., 2015). The Shahejie Formation contains the main source rocks and reservoir rocks, and is divided into three members, Es1, Es2, and Es3 (from top to base) (Fig. 2A). The Es3 member, including five submembers of Es_3^1, Es_3^2, Es_3^3, Es_3^4, Es_3^5 (from top to base), is the main object of this study. The Dongying Formation is divided into three members including the Ed1, Ed2 and Ed3 (from top to base). Regional uplift in the late Oligocene created the unconformity between the Ed and Ng formations. During the uplift stage, the Gaoliu Fault between the GL area and the Liunan subsag led to significant uplift difference between the GL area and other tectonic zones (Fig. 1B) (Guo et al., 2013). In the GL area with great uplift, the total Ed1 and Ed2 and upper part of Ed3 were eroded, whereas in other tectonic zones (eg. Liunan subsag), only the upper part of Ed1 was eroded (Fig. 2A). In the GL area, the Es_3^1, Es_3^2, Es_3^3, Es_3^4, Es_3^5 submembers consist mainly of gray, purple-gray, brownish, and greenish mudstones and interbedded fan delta sandstones deposited in shallow lacustrine environment; the Es_4^3 submember consists mainly of dark-gray oil shale, dark-gray mudstones, calcareous mudstones deposited in a semideep and deep lacustrine environment and gray mudstones with interbedded deltaic fan sandstones deposited in a shallow lacustrine environment (Fig. 2A) (Yuan et al., 2015).

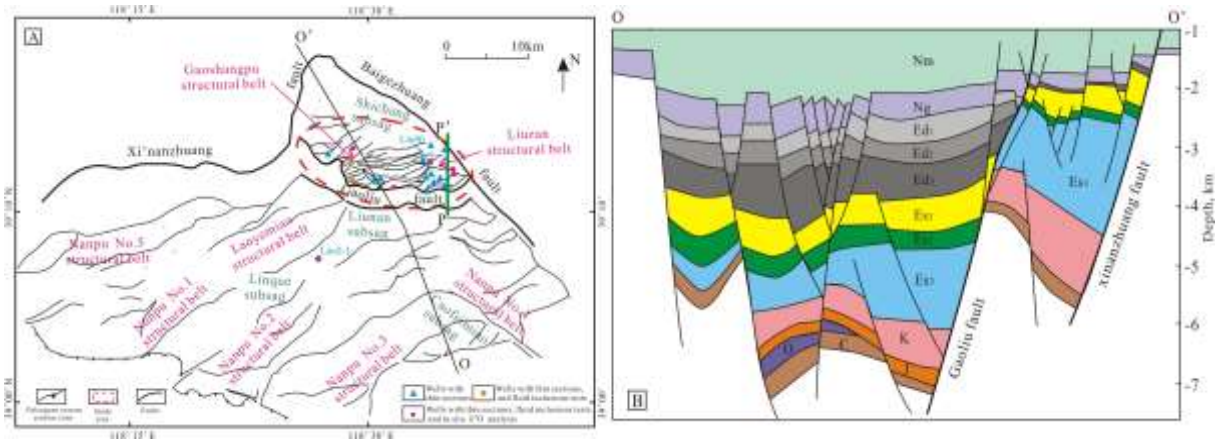

Figure 1. A-Location map of the Gaoliu are (Gaoshangpu structural belt and Liuzan structural belt) in the Nanpu Sag, modified from Yuan et al (2015). B-Cross-section (OO' in Fig.1A) of the Nanpu Sag showing the various tectonic-structural zones and strata in different zones, Modified from Guo et al (2013).

The burial and thermal history of the NP sag has been analyzed in detail using data from exploration and production wells (Fig. 2) (Guo et al., 2013). Present-day geothermal gradient is around 32°C/km, with an average earth surface temperature of 14°C, and maximum burial depth and temperature of the sandstones in the Es3 member occurs today. Due to the tectonic differences, burial and thermal history of sediments in the GL area (Fig. 2A) varies significantly from that of the sediments in the Liunan subsag (Fig. 2B).

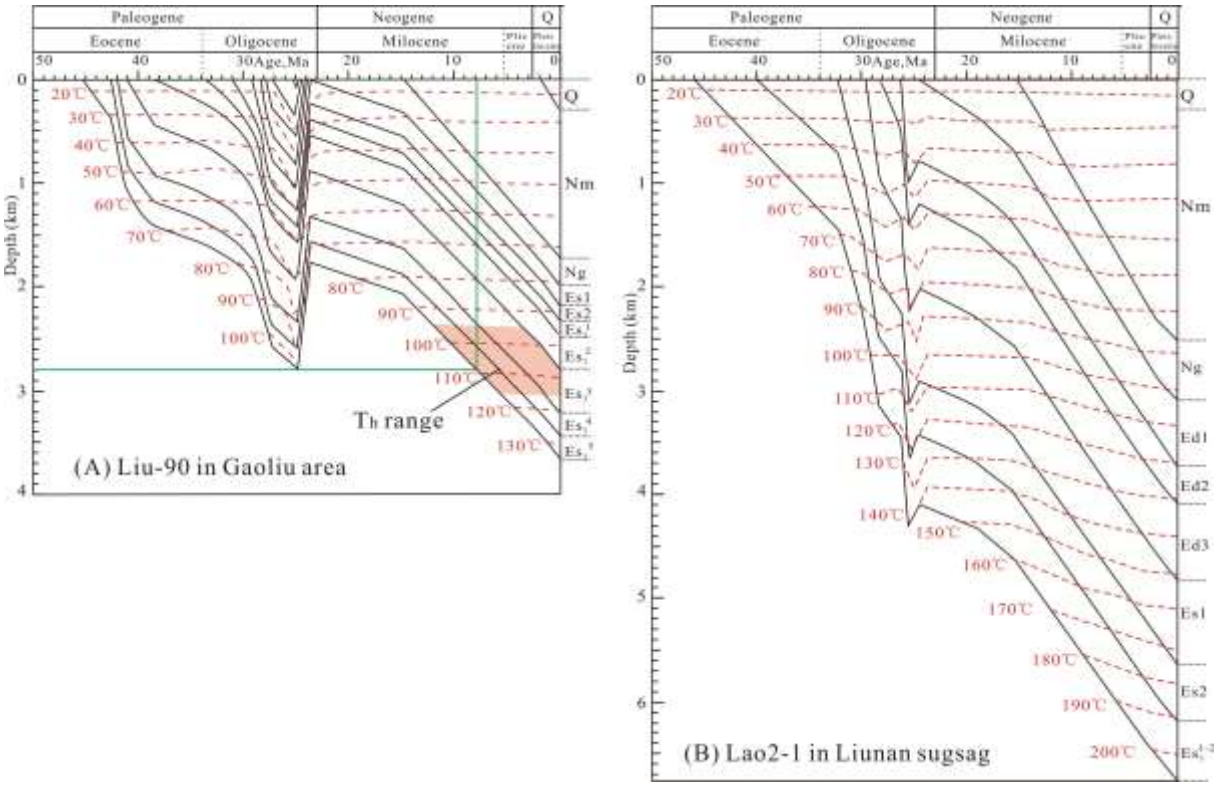

Fig.2 Burial and thermal history of well Liu-90 (A) in the Gaoliu area and well Lao2-1 in Liunan subsag (modified from Guo et al, 2013).

The shadow area in Fig.2A represent the T_h data range of aqueous fluid inclusion in quartz overgrowths; the green lines represent when the studied sandstones were reburied to the maximum depth that has experience during the initial burial stage.

The basin-controlling growth Xi'nanzhaung Fault and Baigezhuang Fault initiated their activity from the early Paleogene period, and the growth Gaoliu Fault initiated its activity from the early Oligocene period. The three faults continued activity until the very end of the Pliocene period (Dong et al., 2008; Li et al., 2010; Zhou, 2000) (Fig.1). These three primary faults are joined by multiple synthetic and antithetic faults

formed during the late Oligocene period to early Neogene period, and these additional faults were active to the end of Pliocene period or even the Quaternary period (Li et al., 2010; Zhou, 2000). In addition, these faults connect the deeply buried Es3 sandstones to shallow strata (Fig. 3) (Yuan et al., 2015).

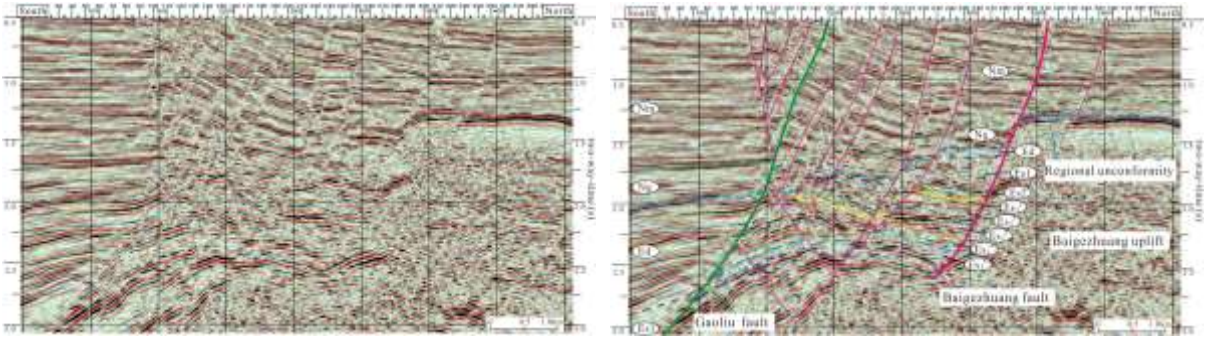

Fig.3 Faults in the Gaoliu area (The north-south Cross section P'P in Fig.1A).

2 Database and Methods

1760 reservoir porosity data of medium-coarse grains sandstones and pebbly sandstones were collected. 117 blue epoxy resin-impregnated thin sections and 40 SEM samples from ES3 cores of 16 wells were analyzed for sandstone petrography, diagenesis and pores, using optical, reflected and cathodoluminescence (CL) microscopy and SEM facility. Quantitative work was conducted on thin sections to obtain the amount of different sandstone compositions and various pores. Point-counts were performed for detrital compositions, and quantative image analysis was conducted for the amount of secondary pores and authigenic cements (Yuan et al., 2015).

Based on identification of the hundreds of thin sections, we picked out 10 rock chips with quartz overgrowths to make 100μm thickness doubly polished sections for fluid inclusion and $\delta^{18}O$ composition analysis. These ten sandstone samples with little clay matrix were collected from 6 drilling cores, with burial depth ranges from 2800m to 4000m. UV light was used to identify aqueous fluid inclusions (AFI). Microthermometry of AFI was conducted using a calibrated Linkam TH-600 stage. The homogenization temperature (T_h) was obtained by cycling. Th measurements were determined using a heating rate of 10 °C/min when temperature was lower than 70°C and a rate of 5 °C/min when temperature exceeded 70 °C. The measured temperature precision for Th is ±1 °C.

Areas of the rocks with substantial quantities of thick quartz overgrowths (25-30um wide) were identified using a microscope. These areas were then cored out from the doubly polished thin sections. The specimens obtained together with standard quartz were mounted into two resin blocks. Micrographs of these two specimen blocks was captured with optical, reflected and cathodoluminescence (CL) microscopy for selection of ion microprobe spots. In situ Secondary ion mass spectrometry (SIMS) oxygen isotopic composition analysis of detrital and authigenic quartz was then conducted on wide quartz overgrowths, using a CAMECA IMS-1280 ion microprobe with a 15-20 um diameter beam, at the institute of Geology and geophysics, Chinese Academy of Sciences (IGGCAS) in Beijing, and the analytical procedures are similar to those reported by Li et al., 2013 (Li et al., 2013). The internal precision of $^{18}O/^{16}O$ ratios is ca 0.2‰ (2 standard deviations, 2SD) from 20 cycles of measurements (Li et al., 2012). The reproducibility of $^{18}O/^{16}O$ ratios by repeated measurements of standard quartz in this study averaged 0.3‰ (2SD).

3 RESULTS

3.1 Sandstone Petrography

Analyzed sandstones are clean moderate-sorted lithic arkoses and feldspathic litharenites, with an

average framework composition of $Q_{30}F_{34}L_{36}$, and less than 1% detrital clays (Tab. 1) (Yuan et al., 2015). The composite diagenetic sequences include compaction and carbonate cementation in eodiagenetic stage, subsequent dissolution of feldspars and early-diagenetic calcite cement, precipitation of some authigenic quartz and kaolinite, and then weak late carbonate cementation in mesodiagenetic stage (Fig.4, Fig.5) (Yuan et al., 2015). The GL sandstone porosity ranges mainly from 4% to 28% (Tab. 1). In tight sandstones with large amount of early-diagentic carbonate cement (Fig.5A), leached feldspars, authigenic quartz and clays are absent. Porous sandstones commonly contain many feldspar pores with small quantities of authigenic quartz, kaolinite and late-diagenetic carbonate cements (Fig.4).

Table.1 average thin-section compositions from optical point counting and quantative image analysis. Detailed data for each sample is available in appendix table-1. '-' not detected, QOF-quartz overgrowths. Intergranular pores including primary and secondary pores formed by calcite leaching

Borehole	TVD(m)	Distances to unconformity, m	n	Quartz	K-feldspar	Plagioclase	Rock fragment	Carbonate cement	Detrital clay	Authigenic kaolinite	QOF	Intragranular Secondary pores in feldspars	Intergranular pores	Core porosity
Gao5	3180-3242	1154-1216	11	29-35	8-16	15-27	29-44	0-25	0.1-10	0-0.2	0-0.02	0.2-4	0-10	8.8-23.9
Gao8x1	3813-3830	1567-1584	11	26-37	19-25	10-13	32-44	0.2-28	1.0-3.0	0-3.5	0	0-0.5	0	5.8-13.8
Gao13	3478-3523	1374-1419	6	24-28	10-15	20-21	37-43	0-2.5	0.2-3	0.2-2	0-0.05	2-3.5	0.2-3	14.5-19.7
Gao23	3560-3597	1595-1632	5	23-26	15-19	20-28	31-42	0-0.5	0.1-0.5	0.1-0.2	0.1-0.3	2.5-5	0.5-3	15.1-20.4
Gao3106	3570-3916	1487-1833	7	23-30	12-20	19-28	31-35	0.1-20	0.1-0.5	0-0.1	0-0.05	0-3	0-7	3.5-19
Liu1-3	2959-2961	907-909	3	25-28	18-26	12-14	32-45	0-0.5	2-3	0.5-2	0.03-0.05	0.5-1	3-7	23.6-26.5
Liu3-3	2957-3073	662-778	4	25-40	10-20	13-15	26-47	0-0.5	0.2-10	0-0.2	0-0.5	0-1	0-2	7-14
Liu12-2	3719-3726	1659-1666	7	25-32	15-20	18-23	33-39	0-5	0-10	0.2-2.5	0-0.05	0.3-2.5	0-1.2	-
Liu15	2624-3521	446-1343	10	28-35	12-18	13-22	30-40	0.2-10	0.1-15	0-1.5	0-0.05	0.05-4	0-8	5.4-32.8
Liu24	2621-3027	449-855	5	28-41	26-35	10-16	8-34	0.2-5	0.2-0.3	0.05-0.1	0-0.1	0.5-1	4-6	15.9-20
Liu160x1	3475-3478	1421-1424	11	18-23	20-22	9-12	44-51	0-4	0.2-12	0-0.2	0-0.05	0-5	0-6	9.6-19.1
Liu68x1	3334-3818	749-1233	7	26-35	15-17	12-18	35-41	0.5-3	0.1-4	0.05-2	0.01-1.5	0.5-2	0-1	-
Liu124x1	2819-3002	648-831	13	26-35	11-21	10-21	27-42	0.2-15	0.2-5	0-0.2	0-0.02	0.2-4	0-10	16.8-17.2
Liu158x1	3310-3361	1424-1475	6	26-31	20-30	10-12	22-43	0-2	0.1-3	0.01-1	0-0.3	0.2-2	1.5-4	9.7-16.8
Liu160x1	2574-2862	688-977	6	32-35	14-20	16-20	29-36	0-20	1-18	0-0.2	0-0.01	0-1	0-10	-
Liushen11	2622-2633	430-441	5	30-46	15-25	8-10	28-37	0-25	0.2-15	0-0.1	0-0.1	0-2	0-10	-

Feldspar diagenesis significantly altered the composition of the sandstones. The feldspars composition, including mainly of detrital K-feldspars grains and K-feldspar in polymineralic rock fragments can be identified to be partially to fully dissolved (Fig.4). Monocrystalline or polycrystalline feldspar grains may be fully dissolved (Fig.A, D), though most feldspars are partly dissolved (Fig.4 C, E). Internal fabric of the feldspar is still recognisable by intricate structures consisting of inherited minerals and secondary pores after the former cleavage or twinning or perthitic structures (Fig.4 C, E). The partial dissolution may be due to varying compositions or limited leaching time, and the remnants can be used to identify dissolution texture. Some detrital plagioclase grains can be identified to be partially leached, but not common. In most cases, the secondary pores after detrital feldspars are not filled with newly formed minerals, showing great different from most other sandstones. The amount of feldspar secondary pores can reach up to 5% of the total rock (Tab.1).

Authigenic quartz can be identified in few thin sections, with amount less than 0.1% of the total rock (Tab.1). Authigenic quartz occurs as syntaxial quartz overgrowths (Fig.4G, H) or small microcrystalline quartz. Thickness of the quartz overgrowths ranges mainly from 2μm to 30μm, whereas size of the quartz

crystals is generally less than 15μm. Quartz overgrowths can be easily identified by dust rim or fluid inclusions at the grain-overgrowth boundary, while microcrystalline quartz can be easily identified in SEM samples. Kaolinite can be identified occasionally in some thin sections and SEM samples, with amount less than 0.5-1.0% in most samples (Tab.1). Kaolinite occurs mainly as vermicular aggregates and anhedral and preudohexagonal plates filling primary pores and a few feldspar pores, and kaolinite aggregates are closely associated thin platelets (Fig.4I).

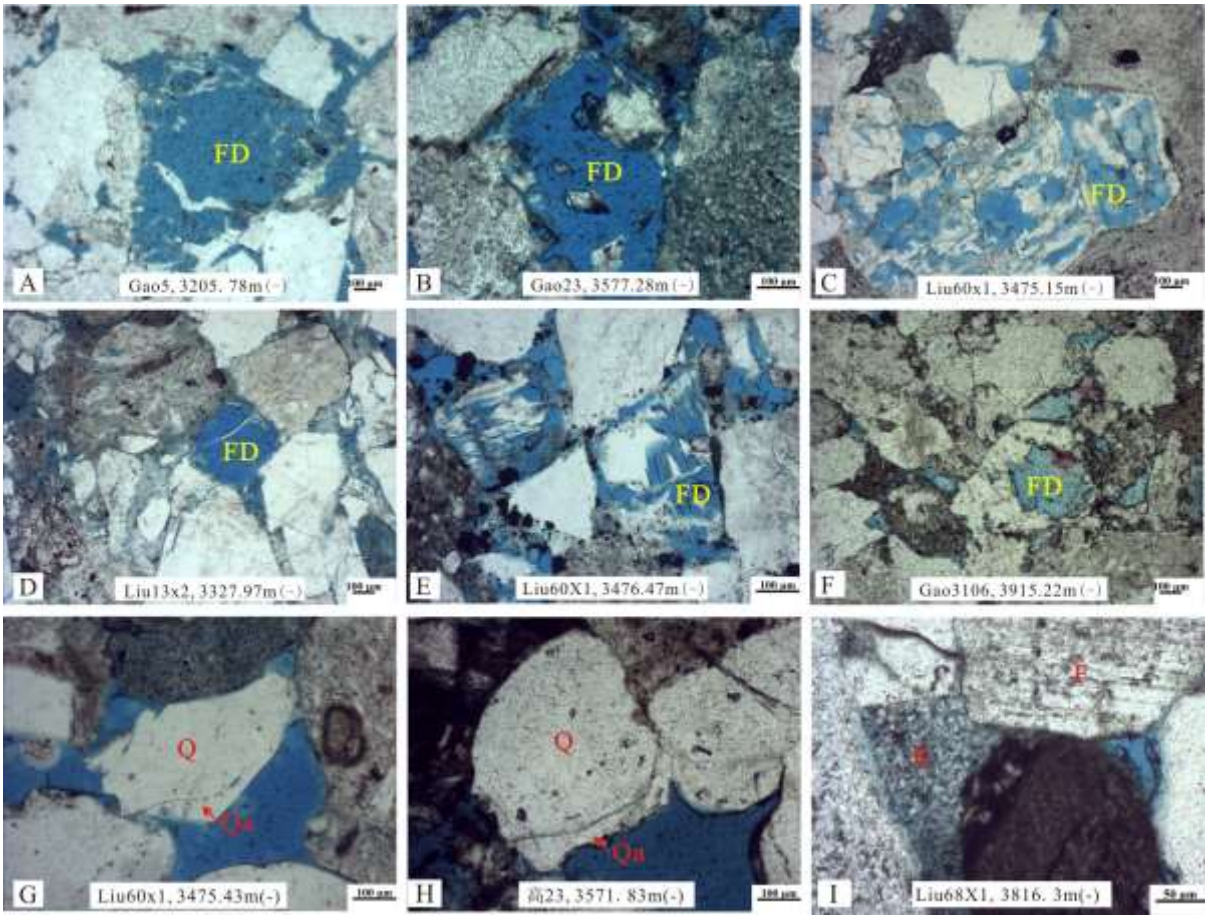

Figure 4. Photomicrographs of leached feldspar and associated secondary minerals in sandstone thin sections. A-F: extensive leached feldspars with little precipitation of secondary minerals in the secondary and pores in most thin sections. Secondary pores after feldspar grains are preserving original outlines of former grains, indicating weak compaction accompanying the leaching reactions. G-H: quartz overgrowths in some few thin sections, quartz overgrowths can be easily identified. I-Kaolinite in some primary pores, blue epoxy resin can be identified in the kaolinite aggregates, indicating the presence of micropores among these plates.

Three types of carbonate cements, early-daigenetic calcite, early-diagenetic dolomite, and late-diagenetic calcite were identified in sandstones (Fig.5). The early-diagenetic calcite occurs as microsparry or sparry interlocking mosaic of crystal, filling primary pores and replaces some detrital grains. In early-diagenetic calcite cemented tight sandstones, the cement occupies almost all primary pores and can account for 25%-30% of the total sandstone volume where leaching of calcite did not occur (Fig.5A). The early-diagenetic calcite appears to be etched in many samples and this is interpreted to indicate that extensive dissolution of such cements occurred in some sandstones (Fig.5C-H). In general, early-diagenetic calcite cemented sandstones or sandstones with extensive dissolution of early-diagenetic calcite cements are usually supported by detrital grains with just point contacts or have a floating texture (Fig.5A, G), indicating little compaction when cementation occurred. Dolomite cement and late-diagenetic calcite can only be identified in a few samples. Late calcite can be identified to fill some secondary pores formed by

feldspar dissolution (Fig.5B), indicating that it is formed after mineral leaching reactions (Fig.2C).

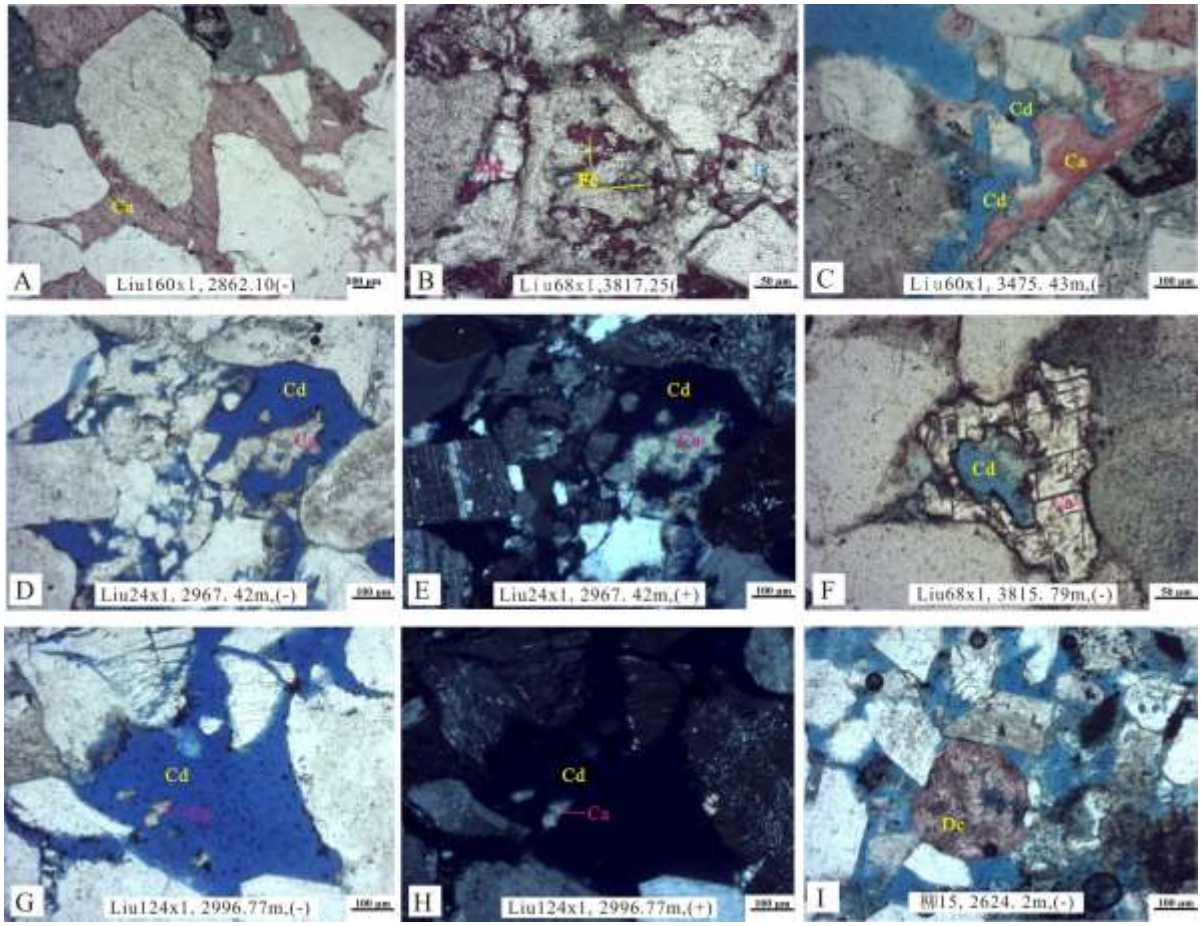

Fig.5 Photomicrographs of carbonate cements and leaching texture of early-diagenetic calcite in sandstone thin sections. A-tight sandstones with large volume of carbonate cements; B-late calcite cements in feldspar pores. C-H: extensive dissolution of early carbonate cements; oversized pores (Fig.5G) indicating weak compaction accompanying the leaching reactions. I: dissolution of detrital calcite grain. D-E and G-H are the same views presented using palne-polarized light and cross-polarized light.

3.2 Fluid inclusions

Secondary fluid inclusions in healed microfractures in quartz grains are abundant (Fig.6B), while primary fluid inclusions in quartz overgrowths are not common (Fig.6A). The size of aqueous fluid inclusions (AFIs) in healed microfractures ranges from 2 to 11 um, and the size of AFIs in quartz overgrowths ranges mainly from 2 to 8 um. The test data show that T_h of AFIs in healed microfractures ranges mainly from 95°C to 125°C. As quartz overgrowths are scarce in reservoirs, only a few AFIs in quartz overgrowths were analyzed, and T_h of these AFIs ranges mainly from 95°C to 115 °C (Tab.2).

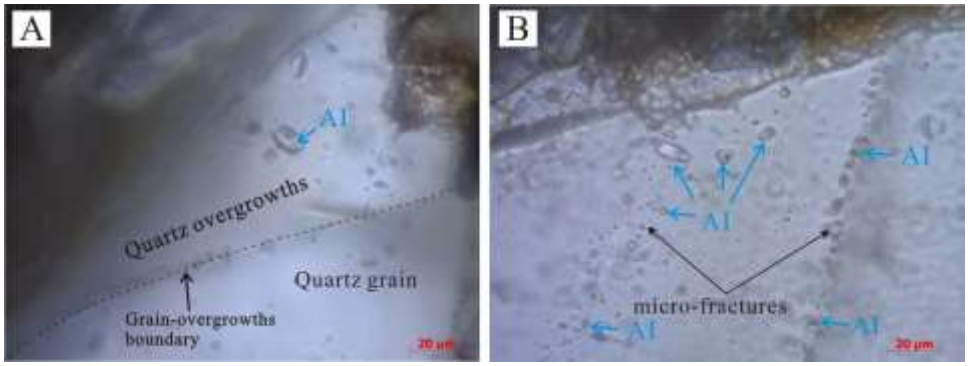

Fig.6 Photomicrographs of aqueous fluid inclusions (AI) under transmitted light observed at room temperature in sandstones from the GL sandstone. (A) Aqueous inclusion within quartz overgrowths; (B) Aqueous inclusions in healed microfractures in quartz grains.

Table 2. Microthermometric data of the aqueous fluid inclusions in the Es3 sandstones. Th: homogenization temperature.

Well	Depth, m	Strata	Distance to unconformity beneath the Ng Formation, m	Aqueous inclusions in healed microfractures in quartz grains		Aqueous inclusions in quartz overgrowths	
				Size, um	Th, °C (Number)	Size, um	Th, °C (Number)
Gao5	3239.67	Es_3^3	1213.67	2-8	95-125 (3)	5	107 (1)
Liu12	3655.77	Es_3^5	1640.27	2-11	107-127(12)	3-8	105-117 (4)
Liu124x1	2996.85	Es_3^4	825.35	2-6	98-115 (6)	3-6	95-105 (2)
Liu24	2895.05	Es_3^4	723.05	3-8	100-109 (5)	6	98-110 (3)
Gao23	3571.83	Es_3^3	1606.83	3-10	102-125 (7)	2-6	103-114 (2)
Gao62	3676.00	Es_3^3	1169	2-9	97-123 (10)	3-6	95-109 (2)

3.3 Oxygen isotope compositions

After ion microprobe analysis was complete, all analysis pits were examined by optical microscope and CL to determine the exact nature of quartz analyzed, that is the approximate proportions of detrital quartz grains and quartz overgrowth. The $\delta^{18}O$ values of the analyzed four rocks are shown in histogram form (Fig. 7). $\delta^{18}O_{(DQ)}$ values within quartz grains ranges mainly from 8‰ to 13‰, and $\delta^{18}O_{(cement)}$ values of pure quartz overgrowths ranges mainly from 17‰ to 20‰.

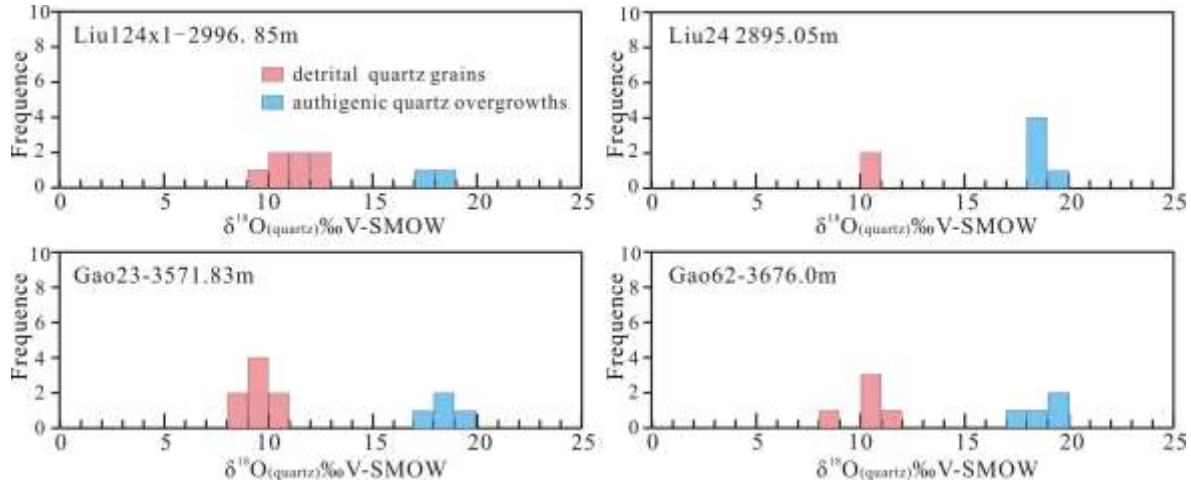

Figure 7. Histograms showing the distribution of $\delta^{18}O$‰V-SMOW values of detrital quartz grains and authigenic quartz overgrowths in four samples.

4 DISCUSSION

4.1 Timing of mineral leaching

The timing of mineral dissolution in sandstones could be early synsedimentary, associated with unconformities, or taking place during later burial (Bjørlykke and Jahren, 2012; Molenaar et al., 2015). With testing of oxygen isotopic compositions, the early-diagenetic calcite cement has been suggested to be precipitated during 40℃-70℃ at relative shallow depth in eodiagenetic stage (Yuan, 2015) , which is also verified by petrography texture of point contacts of detrital grains or floating textures in sandstones with large amount of the early-daigenetic calcite cements (Fig.5A), or oversized pores formed by dissolution of the early-daigenetic calcite cements (Fig.5G). Leaching of such early-diagenetic calcite cements can only occurred after eodiagenetic stage, probably during the uplift

stage and subsequent mesodiagentic stage. The distances of studied samples to the unconformity beneath the Ng formation are generally larger than 800m (Tab.1), which suggest that leaching of such calcite cements occurred at relative deep depth and is irrelevant to the unconformity.

Secondary pores formed by detrital feldspar dissolution did not preserve geochemistry of paleo erosive fluids that can be used for assessing the occurrence of leaching reactions, however, several lines can be used to investigate the relative timing or a range in timing of feldspar dissolution. Firstly, feldspar dissolution occurred mainly in porous sandstones (Fig.4), whereas the tight sandstones with massive early-calcite cements generally contain very limited feldspar pores (Fig.5A), suggesting that the extensive feldspar dissolution occurred mainly after early-calcite cementation . Secondly, oversized pores from early shallow dissolution of grains that developed before the maximus packing density and a collapsed but stable grain framework was reached, would have been destroyed by the observed frame work collapse in deep buried sandstones (Wilkinson et al., 2001), and early formed authigenc clay fabrics would also have been deformed by later compaction. In our studies sandstones (Molenaar et al., 2015), however, the secondary pores after grains are preserving original outlines of former grains (Fig.4A-D), and authigenic kaolinite was not affected by compaction and still has preudohexagonal or vermicular shape (Fig.5I). We do not exclude the early synsedimentary leaching reactions. However, these petrography textures (Fig.4, Fig.5) suggest that feldspar dissolution in the studied sandstones probably mainly occurred after eodiagenetic stage when compaction and early-diagenetic cementation dominated. Results of laboratory leaching experiments in fluids far from equilibrium with feldspars show that the leaching rate constants of feldspars increase by a factor of about ten thousand as temperature increase from 20 °C to 120 °C (Thyne, 2001). Occurring in an open sandstone geochemical system (discussed in Section 4.3), precipitation rate of secondary minerals may has little impact on the leaching reaction (Zhu et al., 2004; Zhu et al., 2010), and the leaching rate of feldspars depends largely on formation temperature. Thus, extensive leaching of feldspars in the studied sandstones probably has been occurring since the uplift stage. As the present pore waters are still undersaturated with respect to the remaining feldspars , the leaching process should be still on.

4.2 Temperature, time and pore water for quartz cementation

As the aqueous fluid inclusions (AFIs) tested in this study were located within the quartz overgrowths, resetting and leakage of these primary AFIs as a result of subsequent burial is unlikely (Girard et al., 2001), which is also verified by the sphere or ellipse shape of these AFIs (Fig.6A). Thus, the T_h data (95-115℃) of the tested fluid inclusions (Tab.2) represent the approximate precipitation temperature of these quartz overgrowths. The T_h data of AFIs in quartz overgrowths was plotted on the burial and thermal history, which suggested that these quartz overgrowths was formed at burial depth of 2500m to 3200m, from approximately 12Ma years ago to 0Ma (Fig.2A).

With constraints of T_h data of AFIs and in situ $\delta^{18}O_{(cement)}$ values (+17～+20‰) within the quartz overgrowths and an quartz-water oxygen isotope fractionation equation (Méheut et al., 2007), oxygen isotopic compositions of paleo-fluids ($\delta^{18}O_{(water)}$) in which quartz overgrowths were formed is calculated to be between -7% to -2‰ (Fig.8). We have reported one coeval closed turbidite sandstone geochemical system with little impact meteoric freshwater in the Shengtuo (ST) area, Dongying Sag, Bohai Bay basin. The diagenetically modified paleo-fluids formed quartz overgrowths at 100-125℃ in the closed geochemical system in the ST area own $\delta^{18}O_{(water)}$ values of 1.5‰-4.5‰ (Yuan et al., 2015). These ST closed sandstones and the GL open sandstones were deposited in the same big basin (Bohai Bay Basin) at similar time, and both sandstones have experienced extensive diagentic reactions (Yuan et al., 2015). The great differences between isotopic compositions of these two paleo-waters and the rather negative$\delta^{18}O_{(water)}$

values of the GL paleo-fluids are hard evidence demonstrating that the quartz cementation in the GL sandstones probably occurred in presence of meteorix water or in diagentic pore water with influence of meteoric water (Aplin and Warren, 1994; Harwood et al., 2013).

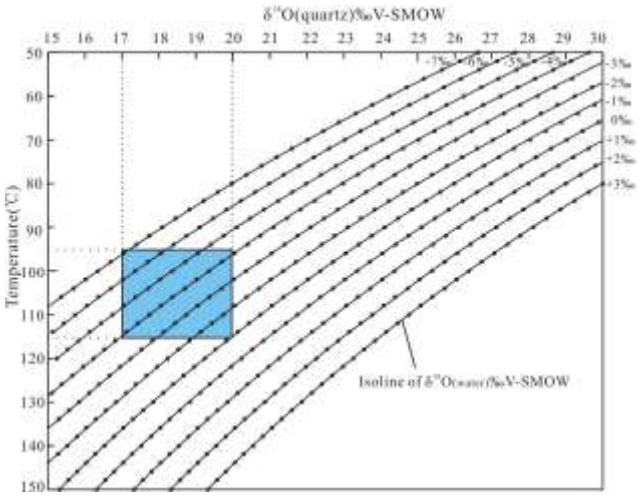

Figure 8. A- Cross plot of $\delta^{18}O_{(quartz)}$ in equilibrium with water ($\delta^{18}O_{(water)}$= -7‰, -6‰, -5‰, -4‰, -3‰, -2‰, -1‰, 0‰, +1‰, +2‰, +3‰) as a function of temperature (Méheut, 2007).

4.3 Open geochemical system for mineral leaching

In closed sandstone geochemical system without large-scale advective flows during deep burial, feldspars are generally leached to form secondary pores and almost equivoluminal in situ secondary minerals including clays (kaoline or illite) and quartz cements (Giles and De Boer, 1990; Higgs et al., 2007; Molenaar et al., 2015). In our studied sandstones, the amount of secondary pores formed by feldspar dissolution can reach up to 3-5% (Tab.1), whereas the kaolinite content is generally less than 0.5-1.0% of the total rock, and no authigenic illite was identified in these sandstones (Tab.1). Quartz cements are generally absent in most samples, though a few samples were identified to contain less than 0.1% quartz overgrowths (Tab.1). The extensive feldspar dissolution provided large amount of Al^{3+}, SiO_2(aq) and K^+, however, only a small portion of these solutes were preserved in the sandstone geochemical system through secondary mineral dissolution. With different compaction rate during burial, connate water in mudstones was expelled to interbedded sandstones as advective flow(Bjørlykke, 1993), thus, transfer of the solutes from sandstones to mudstones can only occur by means of diffusion. Large scale diffusion transfer of Al^{3+} and SiO_2(aq) from sandstones to mudstones is not likely to occur as the reaction of smectite to illite and feldspar dissolution in mudstones also releases Al^{3+} and SiO_2(aq) (Thyne, 2001). The reaction of smectite to illite in mudstones requires potassium, and authigenic illite in mudstones may be a potential sink for potassium derived from the leached K-feldspars in sandstones (Thyne, 2001). However, the concentration of K^+ in pore water in the studied sandstones ranges from 0 to 50 mg/L, with such low solute concentration and concentration gradients, only small amount of K^+ from sandstones to interbedded mudstones could occur by diffusion transfer (Bjørlykke and Jahren, 2012). Massive early-diagenetic calcite cements have been leached (Fig.5), and in most sandstones samples, no late-diagenetic calcite cements were precipitated to preserve the leached solutes. The concentration of Ca^{2+} in pore water should be higher than 10g/L after dissolution of 1% calcite by connate pore water (with supposed salinity of 0) in both sandstones and interbedded mudstones (with mudstone/sandstone ratio less than 5:1 in the GL area), which is much higher than the concentration of Ca^{2+} (generally < 1g/L) in present pore water, indicating extensive export of Ca^{2+}

from the sandstone system.

As large amount of solutes derived from dissolution of feldspars and calcite cements have been removed from the sandstones, we concluded that the mineral leaching reactions probably occurred in open geochemical systems with incursion of large amount of external fluid, and advective transfer of these solutes probably play an important role in exporting such solutes from the GL sandstones.

4.4 Ancient deep incursion of meteoric freshwater

Except the local 200m organic-rich mudstones and shales in the lower part of the Eocene strata, TOC of most other interbedded mudstones in the Eocene formations is generally less than 0.5-1.0%. With the Ro of organic matter ranging from 0.35% to 0.80%, and a mud/sand ratio of 2:1 to 5:1 (Yuan et al., 2015), the organic CO_2 and organic acids generated from maturation of kerogen can account for less than 1-2% of secondary pores in the GL sandstones (Giles and Marshall, 1986; Lundegard et al., 1984). During the uplift period, cooling of hot pore water in the sandstones may dissolve some calcite (Giles and De Boer, 1989). Numerical simulations, however, suggest that cooling of hot fluids retains a very low capacity for dissolving large amounts of calcite in sandstones (Yuan et al., 2015). As leaching of calcite minerals need large amount of acidic water, meteoric freshwater with inorganic CO_2 probably account for such leaching reactions.

Evidence for pressure dissolution of detrital quartz is rather weak in the studies sandstones (Fig.2), and the feldspar dissolution probably provided the silica for the quartz cementation reactions. Two scenarios can be considered for genesis of the quartz cements with high precipitation temperature and low $\delta^{18}O_{(cement)}$ values: (1) the meteoric water got in the sandstones at relative shallow depth during the uplift period but that the cementation reactions did not occur until later burial. That is to say the meteoric water is inherited from freshwater flux during relative shallow burial stage (800-1500m). Or (2) deep incursion of large amount of meteoric water still occurred in the sandstones during subsequent later burial when the cementation reactions took place.

For scenario 1, after the uplift stage, formation temperature increased during the subsequent reburial stage. Without other geological processes seemed to have ceased leaching processes effectively, the temperature increase would lead to increase of feldspar dissolution rate (Thyne, 2001). In such a case, if little freshwater flux occurred in the mesodiagenetic stage, diffusion transfer could not remove the Al^{3+}, SiO_2(aq) released from feldspar dissolution in time, and these solute will be preserved in forms of clays and quartz cements (Giles and De Boer, 1990), which is in conflict with the present petrography textures (Fig.4). Thus scenario 1 cannot satisfactorily explain the observations.

For scenario 2, deep incursion of large scale meteoric water is consistent with the petrography assemblage of extensively leached feldspars with little authigenic kaolinite and quartz cements. Widely developed faults combined the earth's surface and the buried Es3 sandstones (Fig.3B) kept their activity from the late Oligocene period to the end of Pliocene period or even the Quaternary period (Li et al., 2010; Zhou, 2000), may serve as favorable flow conduits for deep penetration of meteoric freshwater to the studied sandstones during the uplift and the reburial period. The significant burial history differences between the GL area and other tectonic zones (eg. Liunan subsag) in the Nanpu Sag (Fig.2) suggests that the Gaoliu area was uplifted more extensively than other tectonic zones during the late Oligocene period, forming a highland in Gaoliu area relative to the Liunan subsag at the declining plate of Gaoliu growth fault. The altitude difference will provide substantial hydraulic drive for deep penetration of meteoric water into these buried sandstones with distance of 800m to 1700m to the unconformity (Bjørlykke, 1993). In the initial burial stage, the studied sandstones have experienced significant compaction with burial depth

ranging from 1800m to approximately 3000m (Fig.2A). Thus, stronger compaction would only occur when burial depth exceeded this depth range in the reburial stage after approximately 8Ma ago, indicating that upward compaction drive flow probably be rather weak during the burial process in the Milocene period. Moreover, various mineral reactions during the reburial stage would consume pore water (Zhang, 2008), which will promote the import of external water to the sandstone system. With combination of these favorable factors, it is very likely that ancient deep incursion of meteoric water could occur in buried sandstones at the depth of approximately 2500-3200m. The low water salinity, low concentration of different ions, the low salinity gradient, and negative hydrogen isotope compositions of present pore waters also indicate that meteoric water must be a vital source of such present waters (Yuan et al., 2015).

4.5 Enhanced secondary pores by burial freshwater leaching

The difference between the amount of feldspar pores and leaching byproducts (kaolinite and quartz cements) show that enhanced porosities formed by feldspar dissolution in the open GL sandstone geochemical system can be up to 3%-4.5% (Fig. 9).

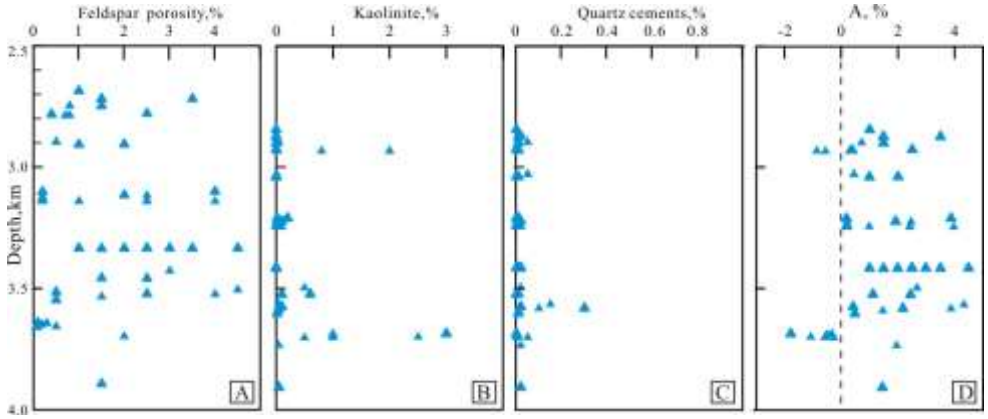

Fig. 9 Vertical variation of the content of feldspar pores, kaolinite and quartz cement and their difference values in thin section in the Gaoliu area (modified from Yuan 2015).

The leaching of early-diagenetic calcite cement is evident in thin sections (Fig.5). Significant negative linear correlations exist between tested core porosity and the amount of carbonate cements in medium-coarse grained sandstones and pebbly sandstones from three different wells (Fig.10), indicating that dissolution of early-diagenetic cement can actually increase reservoir porosity. As burial depth increase, porosity of sandstones with similar amount of carbonate cements does not decrease (Fig.10), indicating that early extensive calcite cementation have retarded compaction effectively, and leaching of such calcite cement released the pore spaces occupied by these cements in the eodiagenetic stage. However, it is difficult to test the amount of these secondary pores formed by calcite leaching using thin sections.

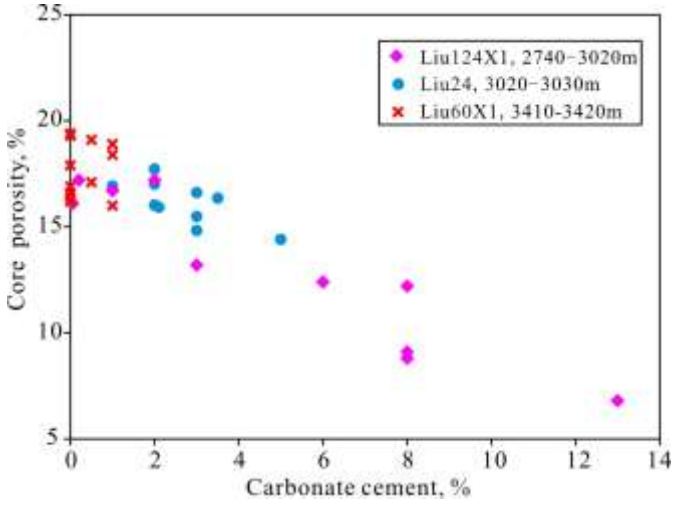

Figure 10. Relationship between core porosity and the amount of carbonate cements in medium- coarse grained sandstones and pebbly sandstones with little clays.

In this study, with constraints of tested core porosity, theoretical porosity-depth trend (compaction curve) from Ramm (1992) (Ramm, 1992), and the enhanced feldspar porosity, secondary porosity formed by leaching of early-diagenetic carbonate cement was estimated. For example, the calculated porosities at depth of 3000m and 3500m were 15% and 12%, respectively. The tested core porosities of sandstones with little clays and calcite cements reach up to 25-28% and 20-22%, respectively (Fig.11). Then, the porosity differences between tested core porosities and calculated porosity range from 10-13% and 8-10% at depth of 3000m and 3500m, respectively. Fluid overpressure does not occur commonly in the studied sandstones, and hydrocarbon emplacement has little impact on porosity of the sandstones with little cements. After deducting the 3-5% porosity enhanced by feldspar dissolution, the remnant porosity differences are 5-8% at 3000m and 3-7% at 3500m, respectively. On condition that most pores have been occupied by early-diagenetic calcite, the porosity released by calcite leaching may be higher than 7-8%.

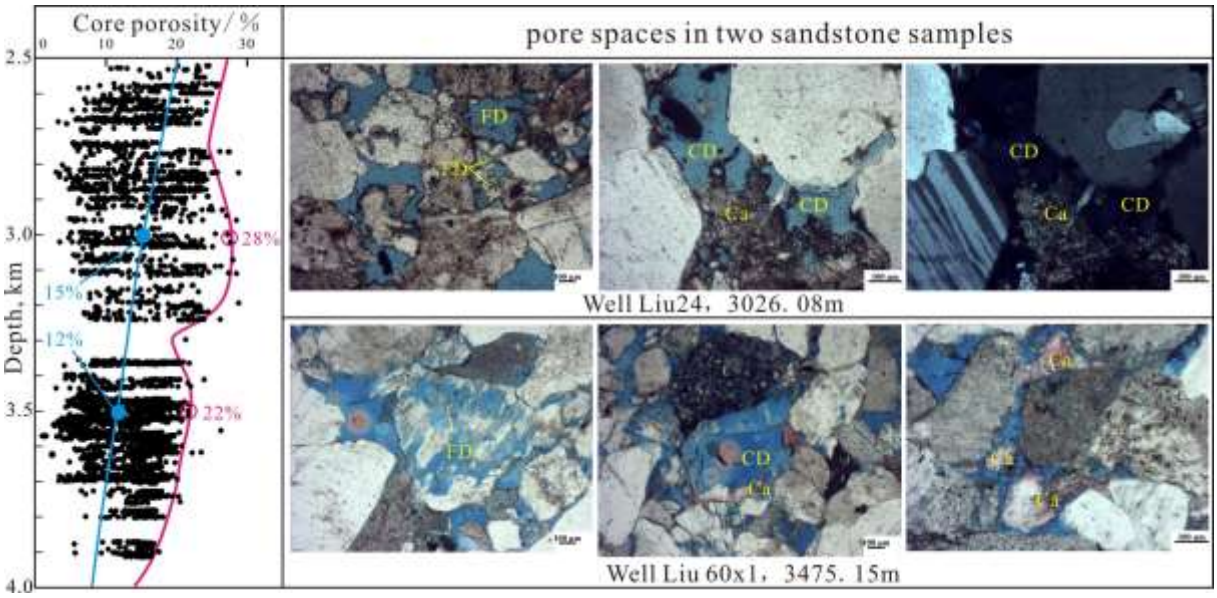

Figure 11. Tested core porosities and calculated porosity curve with a theoretical equation from Ramm (1992). The equation is $\varphi=45e[-(0.23+0.27CFGR)z]$, where CFGR represent the clay content in sandstones, z represents the burial depth.

As large volume of meteoric water can provide inorganic CO_2, the deep meteoric leaching probably can account for the approximated 7%-10% enhanced secondary porosities in these sandstones. Thus, deep meteoric leaching can do improve reservoir quality in open sandstone geochemical system with favorable flow route.

5 CONCLUSION

With valuable authigenic mineral assemblages and geochemical information of paleo-fluids obtained from coupled homogenization temperature (Th) of aqueous fluid inclusions (AFI) and in situ $\delta^{18}O$ compositions within the few quartz overgrowths, we verified the ancient deep incursion of meteoric freshwater in buried open sandstone geochemical system. The studied sandstone in the Gaoliu area, Nanpu Sag is an excellent example showing the significance of deep meteoric leaching in reservoir quality evolution. This knowledge is especially relevant to porosity prediction for petroleum exploration in deeply buried sandstones with developed faults acting as flow route. We emphasize the multidisciplinary

approaches to understanding deep burial meteoric diagenesis in ancient buried sandstone, and we demonstrate the value of geochemistry in defining diagenetic regimes.

ACKNOWLEDGMENTS

This study was funded by the Natural Science Foundation of China Project (No. U1262203), and Foundation for the Author of National Excellent Doctoral Dissertation of China. Jidong Oilfield Company of PetroChina is thanked for supplying all rock samples, blue epoxy resin-impregnated thin sections and some geological data. Doubly polished sections were prepared by Ian Chaplin in Durham University. Petrography and fluid inclusion analysis were made in State key laboratory in China University of Petroleum. Sample preparation and SMIS analysis were assisted by staffs in IGGCAS.

References:

Kevin, P 1995, Diagenesis of Lower Jurassic sandstones, Block 211/13 (Penguin Area), UK northern North Sea: Marine and Petroleum Geology, v. 12, p. 219-228.

Aagaard, P., 1992, Clay minerals in North Sea sandstones: Special Publications, p. 65-80.

Aplin, A.C., and Warren, E.A., 1994, Oxygen isotopic indications of the mechanisms of silica transport and quartz cementation in deeply buried sandstones: Geology, v. 22, p. 847.

Bird, M.I., and Chivas, A.R., 1988, Stable-isotope evidence for low-temperature kaolinitic weathering and post-formational hydrogen-isotope exchange in permian kaolinites: Chemical Geology Isotope Geoscience, v. 72, p. 249-265.

Bjørlykke, K., 1993, Fluid flow in sedimentary basins: Sedimentary Geology, v. 86, p. 137-158.

Bjørlykke, K., and Jahren, J., 2012, Open or closed geochemical systems during diagenesis in sedimentary basins: Constraints on mass transfer during diagenesis and the prediction of porosity in sandstone and carbonate reservoirs: AAPG Bulletin, v. 96, p. 2193-2214.

Dong, Y.X., Wang, Z.C., Zheng, H.J., and Xu, A.N., 2008, Control of strike-slip faulting on reservoir formation of oil and gas in Nanpu sag: Petroleum Exploration & Development, v. 35, p. 424-430.

Dutton, S.P., and Loucks, R.G., 2010, Diagenetic controls on evolution of porosity and permeability in lower Tertiary Wilcox sandstones from shallow to ultradeep (200－6700m) burial, Gulf of Mexico Basin, U.S.A.: Marine and Petroleum Geology, v. 27, p. 69-81.

Emery, D., Myers, K.J., and Young, R., 1990, Ancient subaerial exposure and freshwater leaching in sandstones: Geology, v. 18, p. 1178-1181.

França, A.B., Araújo, L.M., Maynard, J.B., and Potter, P.E., 2003, Secondary porosity formed by deep meteoric leaching: Botucatu eolianite, southern South America: AAPG Bulletin, v. 87, p. 1073-1082.

Giles, M.R., and De Boer, R.B., 1989, Secondary porosity: creation of enhanced porosities in the subsurface from the dissolution of carbonate cements as a result of cooling formation waters: Marine and Petroleum Geology, v. 6, p. 261-269.

Giles, M.R., and De Boer, R.B., 1990, Origin and significance of redistributional secondary porosity: Marine and Petroleum Geology, v. 7, p. 378-397.

Giles, M.R., and Marshall, J.D., 1986, Constraints on the development of secondary porosity in the subsurface: re-evaluation of processes: Marine and Petroleum Geology, v. 3, p. 243-255.

Girard, J., Munz, I.A., Johansen, H., Hill, S., and Canham, A., 2001, Conditions and timing of quartz cementation in Brent reservoirs, Hild Field, North Sea: constraints from fluid inclusions and SIMS oxygen isotope microanalysis: Chemical Geology, v. 176, p. 73-92.

Gluyas, J.G., Robinson, A.G., and Primmer, T.P., 1997, Rotliegend Sandstone Diagenesis: A tale of two waters, Geofluids II 1997: Belfast.

Guo, Y., Pang, X., Dong, Y., Jiang, Z., Chen, D., and Jiang, F., 2013, Hydrocarbon generation and migration in the Nanpu Sag, Bohai Bay Basin, eastern China: Insight from basin and petroleum system modeling: Journal of Asian Earth Sciences, v. 77, p. 140-150.

Harwood, J., Aplin, A.C., Fialips, C.I., Iliffe, J.E., Kozdon, R., Ushikubo, T., and Valley, J.W., 2013, Quartz Cementation History of Sandstones Revealed By High-Resolution Sims Oxygen Isotope Analysis: Journal of Sedimentary Research, v. 83, p. 522-530.

Higgs, K.E., Zwingmann, H., Reyes, A.G., and Funnell, R.H., 2007, Diagenesis, Porosity Evolution, and Petroleum Emplacement in Tight Gas Reservoirs, Taranaki Basin, New Zealand: Journal of Sedimentary Research, v. 77, p. 1003-1025.

Li, H., Jiang, Z., Dong, Y., Wang, X., and Qi, L., 2010, Control of Faults on Hydrocarbon Migration and Accumulation in Nanpu Sag,Bohai Bay Basin: Geoscience, v. 24, p. 755-761.

Li, X., Li, Z., He, B., Li, W., Li, Q., Gao, Y., and Wang, X., 2012, The Early Permian active continental margin and crustal growth of the Cathaysia Block: In situ U – Pb, Lu – Hf and O isotope analyses of detrital zircons: Chemical Geology, v. 328, p. 195-207.

Li, X., Tang, G., Gong, B., Yang, Y., Hou, K., Hu, Z., Li, Q., Liu, Y., and Li, W., 2013, Qinghu zircon: A working reference for microbeam analysis of U-Pb age and Hf and O isotopes: Chinese Science Bulletin, v. 58, p. 4647-4654.

Lundegard, P.D., Land, L.S., and Galloway, W.E., 1984, Problem of secondary porosity: Frio Formation (Oligocene), Texas Gulf Coast: Geology, v. 12, p. 399-402.

Méheut, M., Lazzeri, M., Balan, E., and Mauri, F., 2007, Equilibrium isotopic fractionation in the kaolinite, quartz, water system: Prediction from first-principles density-functional theory: Geochimica et Cosmochimica Acta, v. 71, p. 3170-3181.

Molenaar, N., Felder, M., Bär, K., and Götz, A.E., 2015, What classic greywacke (litharenite) can reveal about feldspar diagenesis: An example from Permian Rotliegend sandstone in Hessen, Germany: Sedimentary Geology, v. 326, p. 79-93.

Ramm, M., 1992, Porosity-depth trends in reservoir sandstones: theoretical models related to Jurassic sandstones offshore Norway: Marine & Petroleum Geology, v. 9, p. 553-567.

Schmidt, V., and McDonald, D.A., 1979, The role of secondary porosity in the course of sandstone diagenesis: SPEM Special Publication, v. NO.26, p. 175-207.

Taylor, T.R., 1996, Association of allochthonous waters and reservoir enhancement in deeply buried Miocene sandstones: Picaroon field, Corsair trend, offshore Texas: in L. J. Crossey, R. Loucks, and M. W. Totten, eds., Siliciclastic diagenesis and fluid flow: Concepts and applications: SEPM Special Publication 55, p. 37-48.

Thyne, G., 2001, A model for diagenetic mass transfer between adjacent sandstone and shale: Marine and petroleum geology, v. 18, p. 743-755.

Wilkinson, M., Haszeldine, R.S., Morton, A., and Fallick, A.E., 2014, Deep burial dissolution of K-feldspars in a fluvial sandstone, Pentland Formation, UK Central North Sea: Journal of the Geological Society, v. 171, p. 635-647.

Wilkinson, M., Milliken, K.L., and Haszeldine, R.S., 2001, Systematic destruction of K-feldspar in deeply buried rift and passive margin sandstones: Journal of the Geological Society, v. 158, p. 675-683.

Yuan, G., Cao, Y., Gluyas, J., Li, X., Xi, K., Wang, Y., Jia, Z., Sun, P., and Oxtoby, N.H., 2015, Feldspar dissolution, authigenic clays, and quartz cements in open and closed sandstone geochemical systems during diagenesis: Typical examples from two sags in Bohai Bay Basin, East China: AAPG Bulletin, v. 99, p.

2121-2154.
Yuan, G., Cao, Y., Jia, Z., Gluyas, J., Yang, T., Wang, Y., and Xi, K., 2015, Selective dissolution of feldspars in the presence of carbonates: The way to generate secondary pores in buried sandstones by organic CO2: Marine and Petroleum Geology, v. 60, p. 105-119.
Yuan, G.H., 2015, Genitic mechanism of dissolution of feldspars and carbonate minerals during diagenesis and its impact on reservoir poroperm (In Chinese with English abstract): Qingdao, China University of Petroleum (East China).
Zhang, S., 2008, “Water Consumption” in the Diagenetic Stage and Its Petroleum Geological Significance: Acta Geologica Sinica, v. 82, p. 663–668.
Zhang, W.C., Li, H., Li, H.J., Meng, Y.L., and Yang, F.B., 2008, Genesis and distribution of secondary porosity in the deep horizon of Gaoliu area, Nanpu Sag: Petroleum Exploration and Development, v. 35, p. 308-312.
Zhou, H., 2000, Relationship between formation, evolution, and hydrocarbona in Nappu Sag: Oil & Gas Geology, v. 21, p. 345-349.
Zhu, C., Blum, A.E., and Veblen, D.R., 2004, Feldspar dissolution rates and clay precipitation in the Navajo aquifer at Black Mesa, Arizona, USA: Water-Rock Interaction, p. 895-899.
Zhu, C., Lu, P., Zheng, Z., and Ganor, J., 2010, Coupled alkali feldspar dissolution and secondary mineral precipitation in batch systems: 4. Numerical modeling of kinetic reaction paths: Geochimica et Cosmochimica Acta, v. 74, p. 3963-3983.